

# Anisotropic pinned/biased magnetization in $SrRuO_3/SrMnO_3$ superlattices

P. Padhan and W. Prellier\*

*Laboratoire CRISMAT, CNRS UMR 6508, ENSICAEN,  
6 Bd du Maréchal Juin, F-14050 Caen Cedex, FRANCE.*

(November 8, 2018)

## Abstract

The exchange coupling at the interfaces of magnetic superlattices consisting of ferromagnetic  $SrRuO_3$  and antiferromagnetic  $SrMnO_3$  grown on (001) oriented  $SrTiO_3$  is studied with in-plane and out-of-plane orientations, with respect to the substrate plane, of the cooling magnetic field. The magnetization of the in-plane, field cooled hysteresis loop is lower than the corresponding in-plane zero-field-cooled hysteresis loop. The out-of-plane field cooled hysteresis loop is shifted, from the origin, along the graphical magnetization axis. We attribute this irreversible rotation of the moment to the pinning/biasing of spin in the  $SrRuO_3$  layer in the vicinity of interfaces by the antiferromagnetic  $SrMnO_3$  layer.

---

\*prellier@ensicaen.fr

The discoveries of novel properties of magnetic films, multilayers and micro- or nanostructures are of high potential to science and technology. The new magnetic phenomena are in the field of nanomagnetism and spin electronics<sup>1</sup> based on multilayers composed of ferromagnetic (*FM*), antiferromagnetic (*AFM*) and non-magnetic, either metallic or insulating, materials. However, the *FM/AFM* multilayers based on 3d - transition metal compounds exhibit overdamped oscillatory exchange coupling<sup>2-4</sup> and unidirectional magnetic anisotropy<sup>5,6</sup>. These two magnetic effects originate from the coupling between the *FM* layers, through the *AFM* layer, and exchange coupling at the *FM* – *AFM* interfaces. The unidirectional magnetic anisotropy is commonly characterized by an exchange field, the field through which the center of the hysteresis loop of the ferromagnet shifts from zero. This phenomenon is generally known as exchange bias. It is usually observed upon cooling the *FM/AFM* system through the Néel temperature  $T_N$  of the *AFM*, to a temperature below the Curie temperature of the *FM* in the presence of a magnetic field. The atomic and magnetic structures at the *AFM/FM* interfaces play a decisive role in the interaction mechanism and thus also for the magnetic properties of the exchange coupled system. The lattice mismatch and strain relaxation can also lead to crystallographic, and/or magnetic reconstructions and relaxations at the interface, which will influence the exchange coupling behavior. The exchange bias phenomenon has been observed in a wide variety of *FM* and *AFM* systems including simple spin structures at the interface to the *FM* layer, such as polycrystalline layers or materials that do not have uncompensated planes of spins in any directions. In general, exchange bias is established through field cooling in-the-film-plane where the magnetic easy axis of soft ferromagnetic materials normally lies in the plane. Recently, Maat *et al.*<sup>7</sup> have shown that exchange bias can also be observed for magnetization perpendicular to the film plane in *Co/Pt* multilayers biased by *CoO*. They investigated the biasing in various directions and found it to be substantially larger within the sample plane, which they related to the anisotropy of the single-q spin structure of the *CoO*.

Most of the previous studies have been performed on metallic compounds, but we have decided to study similar phenomena on transition metal oxide multilayers, grown by laser ab-

lation. Thus, we have synthesized superlattices consisting of ferromagnetic  $SrRuO_3$  ( $SRO$ ) and antiferromagnetic  $SrMnO_3$  ( $SMO$ ) layers, and we report on the structural and magnetic properties of this superlattice system. This magnetic structure exhibits pinned/biased moment below a certain critical field ( $H_P \approx 2$  tesla), and the effects of magnetic fields below  $H_P$  are presented in this article. The pinning effect can be realized in the field-cooled (FC) hysteresis loop. We found that orientation of the cooling magnetic field along the film plane quenches magnetic moments while an out-of-plane cooling field shifts the hysteresis loop, from the origin, along the moment axis. We attribute this irreversible rotation of the moments to the pinning/biasing of spin in the  $SRO$  in the vicinity of the interfaces by the antiferromagnetic  $SMO$ .

A multitarget pulsed laser deposition system was used to prepare the thin films and superlattices of  $SRO$  and  $SMO$  on (001)-oriented  $SrTiO_3$  ( $STO$ ) substrates (lattice parameter  $a_{STO} = 3.905 \text{ \AA}$ ). The thin films and multilayers were deposited at  $720 \text{ }^\circ\text{C}$  in ambient oxygen at a pressure of  $30 \text{ mTorr}$ . The deposition rates (typically  $\sim 0.26 \text{ \AA/pulse}$ ) of  $SRO$  and  $SMO$  were calibrated individually for each laser pulse of energy density  $\sim 3 \text{ J/cm}^2$ . After the deposition, the chamber was filled to  $300 \text{ Torr}$  of oxygen at a constant rate and then the samples were cooled to room temperature at rate of  $20 \text{ }^\circ\text{C/min}$ . The superlattice structures were synthesized by repeating the bilayer comprising of 20-(unit cell,  $u.c.$ )  $SRO$  and  $n$ -( $u.c.$ )  $SMO$ , 15 times, with  $n$  taking integer values from 1 to 20. In all samples, the bottom layer is  $SRO$  and the modulation structure was covered with 20  $u.c.$   $SRO$  to keep the structure of the topmost  $SMO$  layer stable. The periodic modulations in composition were calculated using established deposition rates of  $SRO$  and  $SMO$  obtained from the positions of superlattice reflections in  $X$ -ray  $\theta - 2\theta$  scans. The epitaxial growth and structural characterization of the multilayer and single layer films were performed using  $X$ -ray diffraction (XRD), electron dispersive spectroscopy ( $EDS$ ) and transmission electron microscopy ( $TEM$ )<sup>10</sup>. The magnetization ( $M$ ) measurements were performed using a superconducting quantum interference device based magnetometer ( $Quantum\ Design\ MPMS - 5$ ). The magnetization measurements were carried out by cooling the sample below room tempera-

ture in the presence/absence of magnetic fields along the [100] and [001] directions of the *STO* substrate. The orientation of the magnetic field during the field-cooled measurements remains similar to that of the cooling field.

Fig. 1 shows the (002) reflections of the samples recorded during the  $\theta - 2\theta$  x-ray scans of the thin films of *SRO* and *SMO*, respectively, deposited on (001)-oriented *STO*. The diffraction profiles show only (00 $l$ ) reflections from both the film and substrate, indicating the epitaxial growth of *SRO* and *SMO* on (001)-oriented *STO*. The XRD graph of a 200 *u.c.* thick film of *SRO* is shown in the upper panel (Fig.1a) whereas the lower panel (Fig.1b) shows the scan of a 40 *u.c.* thick film of *SMO* covered with a 10 *u.c.* thick *STO* (this 10 *u.c.* layer of *STO* is only present in order to protect the *SMO* layer). The lattice parameter of bulk *SRO* ( $a_{SRO} = 3.93 \text{ \AA}$ ) is larger than  $a_{STO}$ , with a lattice mismatch of + 0.6 %, whereas the lattice parameter of *SMO* ( $a_{SMO} = 3.805 \text{ \AA}$ ) is smaller than  $a_{STO}$ , with a lattice mismatch of - 2.5 %. The nature of substrate-induced stress for the epitaxial growth of *SRO* and *SMO* on *STO* is the opposite. In our film, this epitaxial correlation is confirmed from the angular positions of *SRO*, *SMO* and *STO* (see Fig. 1).

The  $\theta - 2\theta$  x-ray scans of the superlattices consisting of *SRO* and *SMO* deposited on (001)-*STO* also show the (00 $l$ ) diffraction peaks of both constituents and the substrate, confirming the *c*-axis orientation with a pseudocubic lattice parameter. In Fig. 2 we show the diffracted x-ray intensity with the  $2\theta$  range around the (001) reflection of these pseudocubic perovskite superlattices of (20.*u.c.*)*SRO*/(1.*u.* *SMO*). The presence of second order satellite peaks on either side of the fundamental (001) reflection clearly shows periodic chemical modulation of the constituents. For the quantitative refinement of this sample, we have used the *DIFFaX* program<sup>8</sup> to simulate the diffraction intensity for various diffraction angles. The simulated diffraction profiles of this sample close to the (001) reflection is shown in Fig. 2. The positions and relative intensity ratios of the satellite peaks in the measured  $\theta - 2\theta$  x-ray scan are in good agreement with the simulated profile. The values of the superlattice periods, estimated<sup>9</sup> from the angular position of the satellite peaks in the  $\theta - 2\theta$  x-ray scans, are also in agreement with the calculated value<sup>10</sup>.

$SrRuO_3$  is known as a metallic ferromagnet, with a Curie temperature ( $T_C$ )  $\sim 160$  K in its bulk form<sup>11</sup>. The magnetic properties of a relaxed  $\sim 200$  u.c. thick  $SRO$  film deposited on  $STO$  is shown in Fig. 3. The temperature-dependent magnetization of the film is similar to that of its bulk, while its zero-field-cooled ( $ZFC$ ) magnetic hysteresis at 10 K shows a magnetically easy axis along the [001] direction of the substrate. In the hysteresis loop the saturation magnetization ( $M_S$ ), saturation field ( $H_S$ ) and coercive field ( $H_C$ ), measured along the easy axis of this film, are  $1.46 \mu_B/Ru$ ,  $0.4$  tesla and  $0.17$  tesla, respectively. For the hysteresis loop along the easy axis, the negligibly small difference between the remanent magnetization ( $M_R$ ) and  $M_S$  indicates a coherent rotation of magnetization in a single domain film. As the sample is cooled below room temperature down to 10 K, in the presence of a  $0.1$  tesla magnetic field, the shape of the hysteresis loop is similar to its  $ZFC$  hysteresis loop. In contrast,  $SrMnO_3$  is an antiferromagnet with Neel temperature ( $T_N$ ) close to 260 K<sup>12</sup>, which crystallizes into a cubic structure (Fig. 1b) when sandwiched between perovskite layers inside a superlattice<sup>10,13</sup>.

The low field ( $0.01$  tesla) temperature dependent  $ZFC$  and  $FC$  magnetizations of the sample with  $n = 1$  are shown in Fig. 4(a). The  $ZFC$  magnetization with in-plane magnetic field increases slowly when heated above 10 K, reaching a maximum at  $\sim 150$  K and then decreasing slowly upon further heating to room temperature. The  $FC$  magnetization, with a  $0.01$  tesla cooling field, remains the same when heated from 10 K up to  $\sim 50$  K. Upon further heating, the magnetization decreases slowly and then rapidly in the temperature range of 100 K to 160 K. Above 160 K the value of magnetization is close to that of its  $ZFC$  value. The large difference in the  $ZFC$  and  $FC$  magnetizations below 160 K suggests freezing of the moments of  $SRO$  by the  $SMO$  in the  $ZFC$  state. The low field temperature dependent magnetization along [100] and [001] directions of the substrate for the sample with  $n = 4$  is shown in Fig. 4(b). In this magnetic structure, the alternate stacking of  $SRO$  and  $SMO$  leads to the magnetic inhomogeneity along the [001] direction of the substrate, which may lead to the low field anisotropy in the magnetization along the [100] and [001] directions of the substrate. Another possible source of the low field anisotropy could be due

to the observed anisotropy in the SRO layer (Fig. 3b). To establish the origin of these two effects we have measured the field dependent ZFC and FC magnetizations of these samples at 10 K. The hysteresis loops are shown in Fig. 5. The measurements are based on two aspects: firstly by the response of the magnetic anisotropy of the sample to the direction of magnetic field, and secondly by the effect of a cooling field on the magnetic configuration of the sample.

The *ZFC* hysteresis loop measured in the field range of  $\pm 1$  tesla (larger than the saturation field of *SRO*) shows lower values of  $M_R$  and  $H_C$  compared with the thin film of *SRO* (Fig. 3b). The magnetization increases gradually as the magnetic field increases and the hysteresis loop does not reveal a distinct  $H_S$  and  $M_S$ . The *ZFC* hysteresis loops with a magnetic field oriented along the [100] and [001] directions of the substrate for the sample with  $n = 2$  are shown in Fig. 5(a). The loop shape indicates that the effect of *AFM SMO* on the magnetic configurations of *SRO* is stronger for a field perpendicular to the film plane. The in-plane hysteresis loop is symmetric with respect to the magnetization as well as the field axis, while the out-of-plane hysteresis loop is symmetric along the field axis, with a negligibly small shift along the magnetization axis. This shift of the hysteresis loop from the origin along the magnetization axis is due to the presence of a small magnetic field remaining from when the sample was cooled below room temperature. This intrinsic effect is clearer when the sample is cooled to 10 K below room temperature in the presence of a magnetic field.

The in-plane *ZFC* and *FC* hysteresis loops for the sample with  $n = 3$  are shown in Fig. 5(b). These hysteresis loops are symmetric with respect to the field and the magnetization axis (graphical axis). The magnetization of the in-plane *ZFC* hysteresis loop decreases as the sample is cooled below room temperature in the presence of 0.1 tesla magnetic field. However, a similar effect is not observed for the out-of-plane *ZFC* and *FC* hysteresis loops. On cooling below room temperature down to 10 K in the presence of a 0.1 tesla magnetic field the out-of-plane hysteresis loop at the SRO/*SMO* superlattices shifts, from the origin, along the magnetization axis. The out-of-plane *ZFC* and *FC* hysteresis loops of the superlattice

with  $n = 5$  and  $10$  are shown in Fig. 5(c) and 5(d), respectively. The values of  $H_C$  are equal and opposite for both the increasing and decreasing branches of the  $FC$  loops whereas the values of  $M_R$  are different with the same sign. The magnetization of the  $FC$  loop increases gradually as the magnetic field increases and neither reveal a distinct  $H_S$  nor  $M_S$ .

The magnetic interaction across the interface between an  $FM$  spin system and an  $AFM$  spin system is known as exchange coupling. This interfacial magnetic coupling depends strongly on the spin configuration at the  $FM - AFM$  interfaces, which occurs due to the crystallographic, and/or magnetic reconstructions, and relaxations at these interfaces. In SRO/SMO superlattices we have observed the variation of relaxation at the SRO-SMO interfaces with the SMO layer thickness<sup>10</sup>. Thus the magnetic coupling and the spin configuration at these interfaces of  $FM$  SRO and  $G$ -type  $AFM$  SMO, depend on the SMO layer thickness. When the SMO layer thickness is 1 u.c., the interfacial spin configuration is associated with the 3D-coordination of  $RuO_6$  and  $MnO_6$  and the in-plane staggered pattern spin arrangement in SMO. This is the source of spin frustration at the SRO/SMO interfaces as well as the spin canting in the SRO layer in the vicinity of these interfaces. However, as the SMO layer thickness increases above 1 u.c. the interface spin arrangement is influenced by another component due to the staggered pattern spin in SMO along the  $(00l)$  planes. In other words, above 1 u.c. the interface spin arrangement is influenced by the in-plane and out-of-plane staggered patterns. The increase of the  $(00l)$  planes in SMO increases spin canting in the SRO and saturate for the higher values of SMO layer thickness. A similar effect is observed for the magnetic moment of the superlattice for various SMO layer thicknesses.

Since the  $T_C$  of SRO is smaller than the  $T_N$  of SMO when cooling the superlattices below room temperature, the exchange coupling at the interfaces will vary at different temperature zones. At the interfaces the exchange between the transition metal ions, when both the materials are paramagnetic ( $PM$ ) at room temperature, changes as SMO becomes AFM (at  $T_C < T < T_N$ ) and SRO becomes FM (at  $T < T_C$ ). At  $T < T_C$  the coupling energy at the interfaces between SRO and SMO layers is proportional to the magnetic field<sup>14</sup>. Thus,

the spin configurations of the *SRO/SMO* superlattices are influenced by the magnetic field, its orientation and the thermal energy during the *FC* state. Therefore, a difference can be expected in the coupling energy at the interfaces in the *FC* and *ZFC* state. However, in this superlattice the strength and nature of coupling depend on the orientation of the magnetic field. Assuming that the bulk spin configuration is preserved<sup>5</sup>, we have considered that the *SMO* is rigid with respect to the orientation at low field ( $< 2$  tesla) and the moments lie in-the-plane of the film. According to this assumption the spin configuration of the superlattices are in-plane when the magnetic field is along the [100] direction while the spins of *SRO* and *SMO* are oriented perpendicular to each other for the magnetic field along the [001] direction of the substrate. Since the anisotropy axis of *SMO* is fixed, the magnetic field along the easy axis of *SMO* decreases the angle between the magnetization of *SRO* and the easy axis of *SMO* while their angular separation increases as the magnetic field rotates by  $90^\circ$ . For both orientations, the magnetic field leads to different Zeeman energies, and this could be the source anisotropy (quenching of the in-plane moment and shifting of the out-of-plane hysteresis loop from the origin along the moment axis). The spins close to the interfaces in *SRO* are canted<sup>15</sup>, and their rotations are reversible as seen in the *ZFC* hysteresis loop, but when the cooling field is applied, the coupling energy increases leading to an irreversible rotation below the critical magnetic field. We attribute this irreversible rotation of the moment to the pinning/biasing of spin in the *SRO* in the vicinity of interfaces by the *AFM SMO*.

In conclusion, we have observed pinned/biased moment in the *FM/AFM* superlattices consisting of a ferromagnetic *SRO* and antiferromagnetic *SMO* bilayer. The magnetization of the *FM SRO* layer is suppressed in the *SRO/SMO* superlattices. We attribute this to the randomly pinned/biased moments in the *SRO* layer in the vicinity of the interfaces due to the strong exchange coupling at the *SRO-SMO* interfaces. These superlattices show a shift of the out-of-plane *ZFC* hysteresis loop, from the origin, along the magnetization axis, whereas the magnetic moment quenches the in-plane hysteresis loop. This anisotropic



effect can be viewed as the oriented (*FM* or *AFM*) pinning/biasing of moments in the *SRO* in the vicinity of the interfaces caused by the cooling field. The exchange coupling between the *SRO* and *SMO*, due to the modified 3*D*-coordination of *Mn* and *Ru* ions and the anisotropic nature of *SMO*, are responsible for anisotropic pinned/biased moments with the orientations of the magnetic field. As our understanding of the phenomena at the interfaces of magnetic multilayers is growing, it is hoped that these results may bring new insights about such important issues.

Acknowledgments:

We thank Prof. B. Mercey for the helpful discussions. We also thank Dr. H. Eng for his careful reading of this article. We greatly acknowledge the financial support of the Centre Franco-Indien pour la Promotion de la Recherche Avancee/Indo-French Centre for the Promotion of Advance Research (CEFIPRA/IFCPAR) under Project N°2808-1.

## REFERENCES

- <sup>1</sup> S.A. Wolf, D.D. Awschalom, R.A. Buhrman, J.M. Daughton, S. von Molnar, M. L. Roukes, A.Y. Chtcheelkanova, and D.M. Treger, *Science* 294, 488 (2001).
- <sup>2</sup> A. Orozco, S.B. Ogale, Y.H. Li, P. Fournier, Eric Li, H. Asano, V. Smolyaninova, R.L. Greene, R.P. Sharma, R. Ramesh and T. Venkatesan, *Phys. Rev. Lett.* 83, 1680 (1999).
- <sup>3</sup> K.R. Nikolaev, A. Yu. Dobin, I.N. Krivorotov, W.K. Cooly, A. Bhattacharya, A.L. Kobrinskii, L.I. Glazman, R.M. Wentzovitch, E. Dan Dahlberg and A.M. Goldman, *Phys. Rev. Lett.* 85, 3728 (2000).
- <sup>4</sup> P. Padhan, R.C. Budhani and R.P.S.M. Lobo, *Europhys. Lett.* 63, 771 (2003).
- <sup>5</sup> J. Nogués, and I. K. Schuller, *J. Magn. Magn. Mater.* 192, 203 (1999).
- <sup>6</sup> I. Panagiotopoulos, C. Christides, M. Pissas and D. Niarchos, *Phys. Rev. B* 60, 485 (1999).
- <sup>7</sup> S. Maat, K. Takano, S.S.P. Parkin, and E.E. Fullerton, *Phys. Rev. Lett.* 87, 087202 (2001).
- <sup>8</sup> [http://ccp14.sims.nrc.ca/ccp/ccp14/ftp-mirror/diffax/pub/treacy/DIFFaX\\_v1807/](http://ccp14.sims.nrc.ca/ccp/ccp14/ftp-mirror/diffax/pub/treacy/DIFFaX_v1807/)
- <sup>9</sup> E.E. Fullerton, I.K. Schuller, H. Vanderstaeten and Y. Bruynseraede, *Phys. Rev. B* 45, 9292 (1992).
- <sup>10</sup> P. Padhan, W. Prellier, and B. Mercey, *Phys. Rev. B* 70, 184419 (2004), [cond-mat/0408513](https://arxiv.org/abs/cond-mat/0408513).
- <sup>11</sup> G. Cao, S. McCall, M. Shepard, J. E. Crow, and R. P. Guertin, *Phys. Rev. B* 56, 321 (1997).
- <sup>12</sup> T. Takeda and S. Ohara, *J. Phys. Soc. Jpn.* 37, 275 (1974).
- <sup>13</sup> P.A. Salvador, A.M. Haghiri-Gosnet, B. Mercey, M. Hervieu, and B. Raveau, *Appl. Phys. Lett.* 75, 2638 (1999).
- <sup>14</sup> W.H. Meiklejohn, *J. Appl. Phys.* 33, 1328 (1962).

<sup>15</sup> M. Izumi, Y. Ogimoto, Y. Okimoto, T. Manako, P. Ahmet, K. Nakajima, T. Chikyow, M. Kawasaki, and Y. Tokura, Phys. Rev. B 64, 064429 (2001).

Figure captions:

Fig. 1: X-ray diffraction profiles of the samples recorded around the 002 reflection of *STO*. (a) 200 *u.c.* *SRO* on *STO* and (b) bilayer of (10 *u.c.*)*STO*/(40 *u.c.*)*SMO* on *STO*.

Fig. 2: Measured and simulated  $\Theta - 2\Theta$  spectra for (20 *u.c.*)*SRO*/(1 *u.c.*) *SMO* superlattice around the (001) reflection of *STO*.

Fig. 3(a) *FC* magnetization of the (200 *u.c.*)*SRO* on *STO* at different temperatures with a 0.1 *tesla* in-plane magnetic field. (b) Isothermal (10 *K*) magnetization (*ZFC* and *FC*) of the (200 *u.c.*)*SRO* on *STO* with various fields oriented along the [100] and [001] directions of the *STO* substrate.

Fig. 4(a) *ZFC* and *FC* magnetization of the superlattice with  $n = 1$  at different temperatures with a 0.1 *tesla* in-plane magnetic field. (b) *FC* magnetization of the superlattice with  $n = 4$  at different temperature at 0.1 *tesla* magnetic field oriented along the [100] and [001] directions of the *STO* substrate.

Fig. 5(a) *ZFC* magnetization of the superlattice with  $n = 2$  at 10 *K* with various magnetic fields oriented along the [100] and [001] directions of the *STO* substrate. (b) *ZFC* and *FC* magnetization of the superlattice with  $n = 3$  at 10 *K* with various in-plane magnetic fields. (c) and (d) *ZFC* and *FC* magnetization of the superlattice with  $n = 5$  and 10, respectively, at 10 *K* with various out-of-plane magnetic fields.

Fig. 1  
Padhan & Prellier

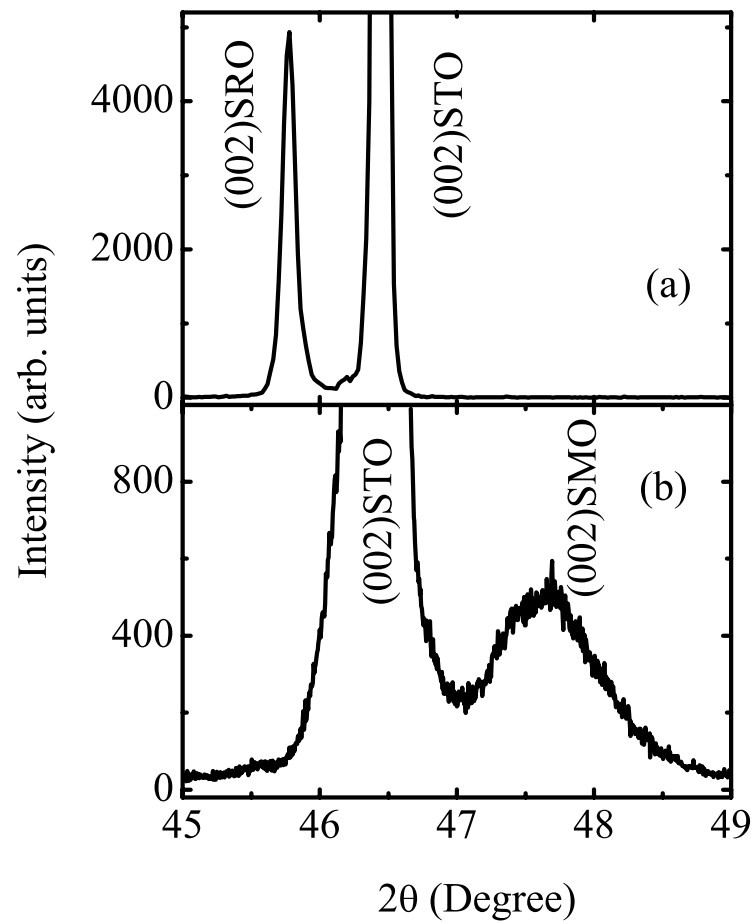


Fig. 2  
Padhan & Prellier

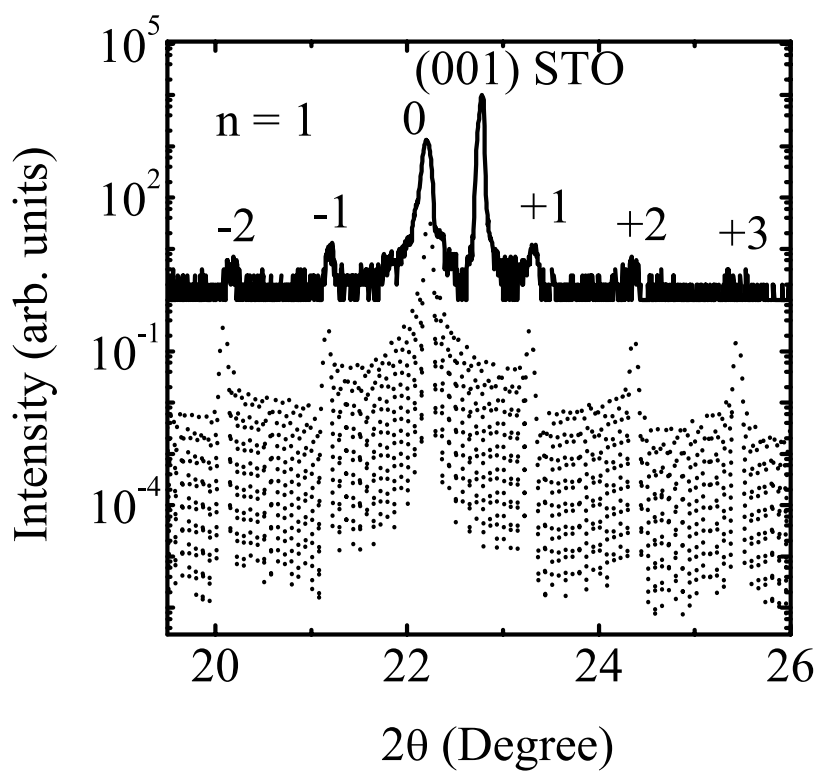


Fig. 3  
Padhan & Prellier

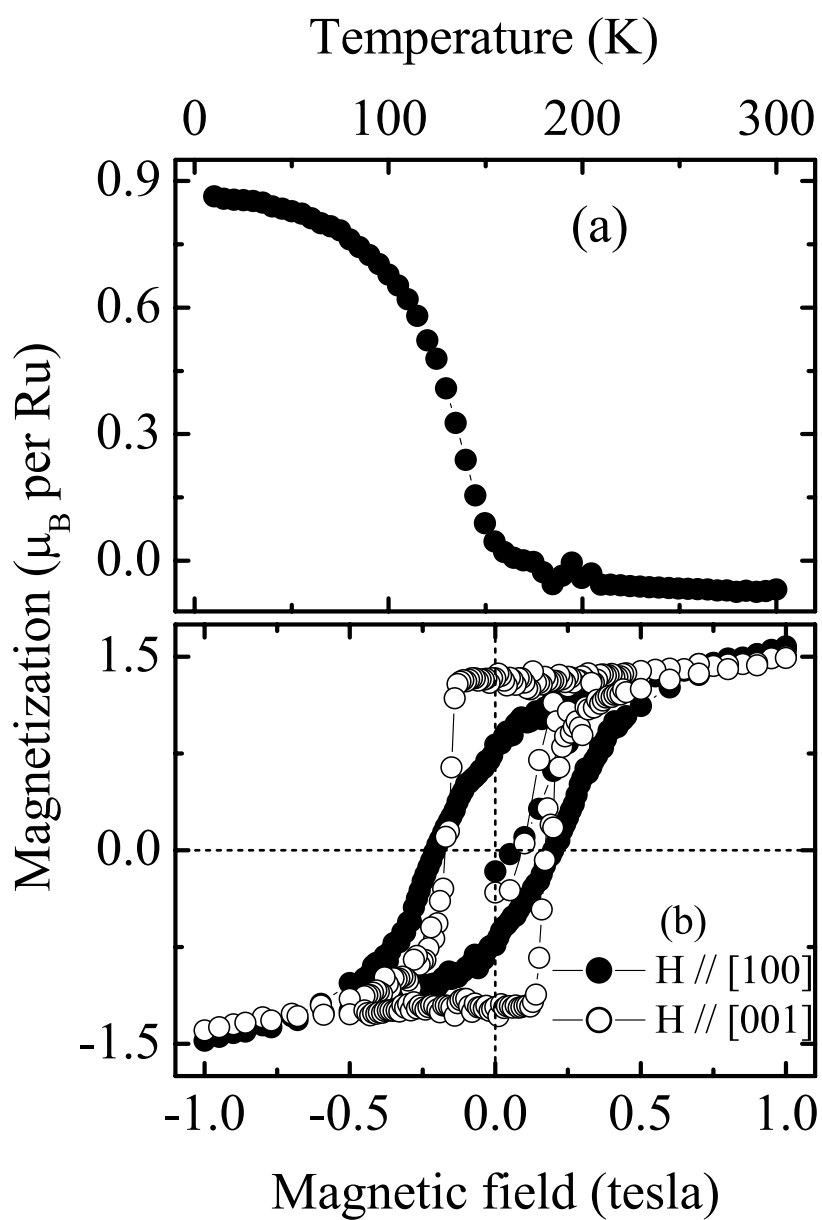


Fig. 4  
Padhan & Prellier

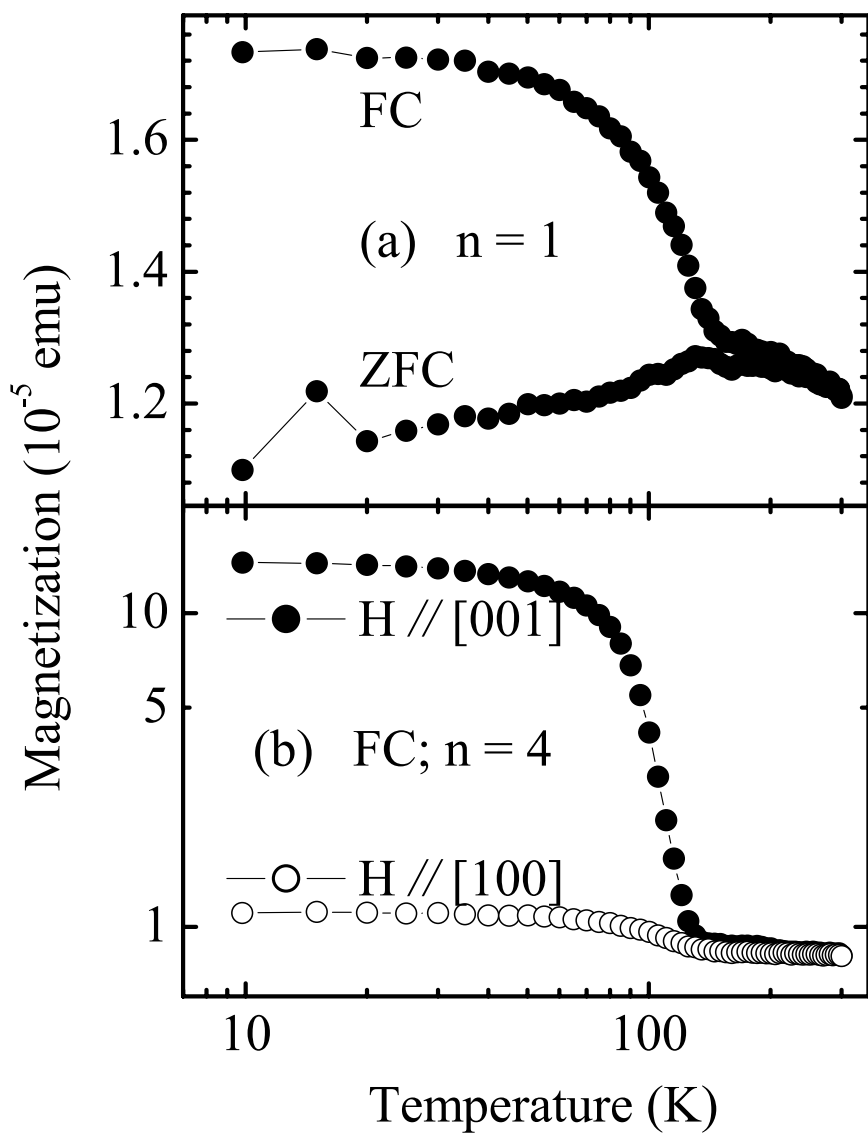




Fig. 5  
Padhan & Prellier

